



# Postglacial evolution of the Lake Constance shelf and its relation to a 10-km long chain of submerged Neolithic mounds

Dominic Perler · Simone Benguerel · Hansjörg Brem · Florence Gilliard ·  
Jens Hornung · Thomas Keiser · Urs Leuzinger · Sebastian Schaller ·  
Sönke Szidat · Hendrik Vogel · Martin Wessels · Flavio S. Anselmetti

Received: 28 August 2023 / Accepted: 22 March 2024  
© The Author(s) 2024

**Abstract** A recent bathymetric survey of Lake Constance revealed ~170 mounds composed of loosely deposited rocks aligned in a ~10-km long chain along the southern Swiss shoreline in a water depth of 3–5 m. The mounds are 10–30 m in diameter and up to 1.5 m high. Over their entire length of occurrence, the mounds are estimated to be

composed of ~60 million individual boulders, with a total weight of ~78,000 t. A ground penetrating radar (GPR) survey showed that the mounds are not linked to the glacial substrate but were rather deposited artificially on the edge of a prograding shelf composed of Holocene lake sediments. Here, we present the results of a coring campaign with four piston cores along a GPR transect across one of the mounds. The cores recovered the full Holocene sedimentary succession all the way into the basal till that is overlain by lacustrine sediments dating back to ~14,400 cal. yrs BP. The four cores are merged into a ~12.4-m long composite section reflecting continuous sedimentation from the siliciclastic-dominated Late Glacial to the carbonate-rich Late Holocene. The stratigraphic horizon representing the mound's construction was radiocarbon-dated to ~5600–5300 cal. yrs BP, placing them in the Neolithic period. This age was confirmed by radiocarbon dating of wood samples collected during underwater excavation of the mounds. Geochemical analysis of the Holocene sedimentary succession shows generally high carbonate contents (average of 69%). The interval from 5750 to 4950 cal. yrs BP, a part of the mound period, is characterized by a Holocene minimum in carbonate content (average of 57%) and by larger mean grain sizes. Comparing these values to those from a recent surface-sediment depth transect indicates that this was a period of rather low lake levels, which might have favoured mound construction. Correlations to nearby archaeological

**Supplementary Information** The online version contains supplementary material available at <https://doi.org/10.1007/s10933-024-00322-2>.

D. Perler (✉) · S. Benguerel · S. Schaller · H. Vogel ·  
F. S. Anselmetti

Oeschger Centre for Climate Change Research, Institute of Geological Sciences, University of Bern, Baltzerstrasse 1+3, 3012 Bern, Switzerland  
e-mail: d.perler@hotmail.com

S. Benguerel · H. Brem · F. Gilliard · T. Keiser ·  
U. Leuzinger  
Departement für Erziehung und Kultur, Amt für Archäologie, Kanton Thurgau, Frauenfeld, Switzerland

S. Benguerel · J. Hornung  
Institut für Angewandte Geowissenschaften, Technische Universität Darmstadt, Darmstadt, Germany

S. Benguerel · M. Wessels  
Institut für Seenforschung der LUBW, Langenargen, Germany

S. Benguerel · S. Szidat  
Department of Chemistry, Biochemistry and Pharmaceutical Sciences, Oeschger Centre for Climate Change Research, University of Bern, Bern, Switzerland

sites and to the general West-Central European lake-level record indicates that the mounds likely were built during a short phase of low lake levels during a general trend of climatic cooling followed by a lake-level transgression.

**Keywords** Lake sediments · Lake-level changes

## Introduction

From 2013 to 2015, the International Commission for the Protection of Lake Constance (IGKB) supported a bathymetric survey of Lake Constance. A combination of multibeam echo sounding (MBES) and airborne laser scanning (LiDAR) resulted in a new high-resolution bathymetric map covering the whole lake with a grid resolution of 0.5 m (not public), as well as 3 m and 10 m, which are available

to the public. Within the first analyses of the results, a chain of submerged mounds along the shallow-water zone of the southern shore in Switzerland was discovered (Wessels et al. 2016). This initial, unexpected discovery laid the base for a systematic exploration by the Archaeological Department of the Canton of Thurgau (AATG): the mounds are arranged parallel to the shoreline in a water depth of 3–5 m with a regular spacing of 85–110 m. The whole chain of mounds stretches from the village of Altnau to the town of Romanshorn, covering ~10 km (Fig. 1). The mounds are circular in shape with diameters of 10–30 m and a height of up to 1.5 m. They are built up by loosely deposited, cobble-sized rocks, which reflect the composition of local outcrops of till sediments in creeks and along the beach, consisting mainly of Molasse sandstones with minor amounts of gneisses, limestones and other crystalline rocks (Leuzinger et al. 2021). The total chain is estimated to

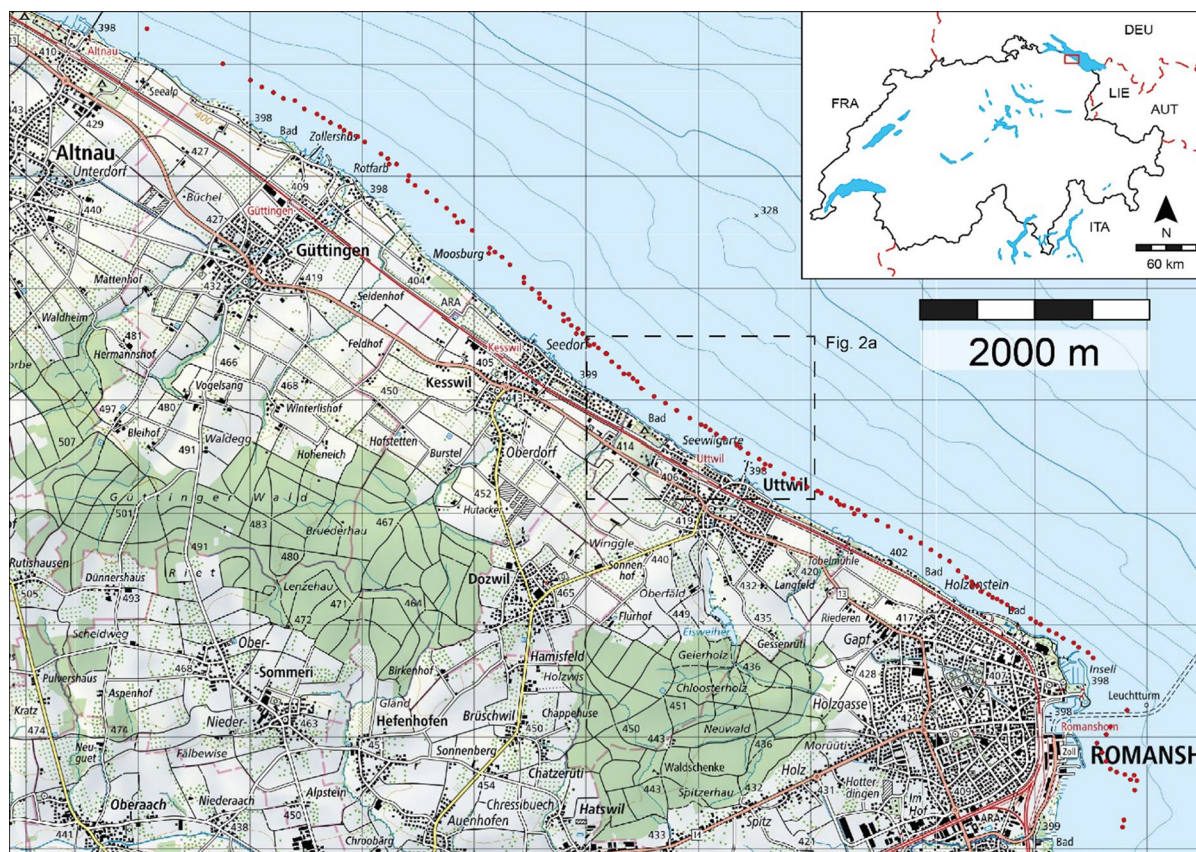
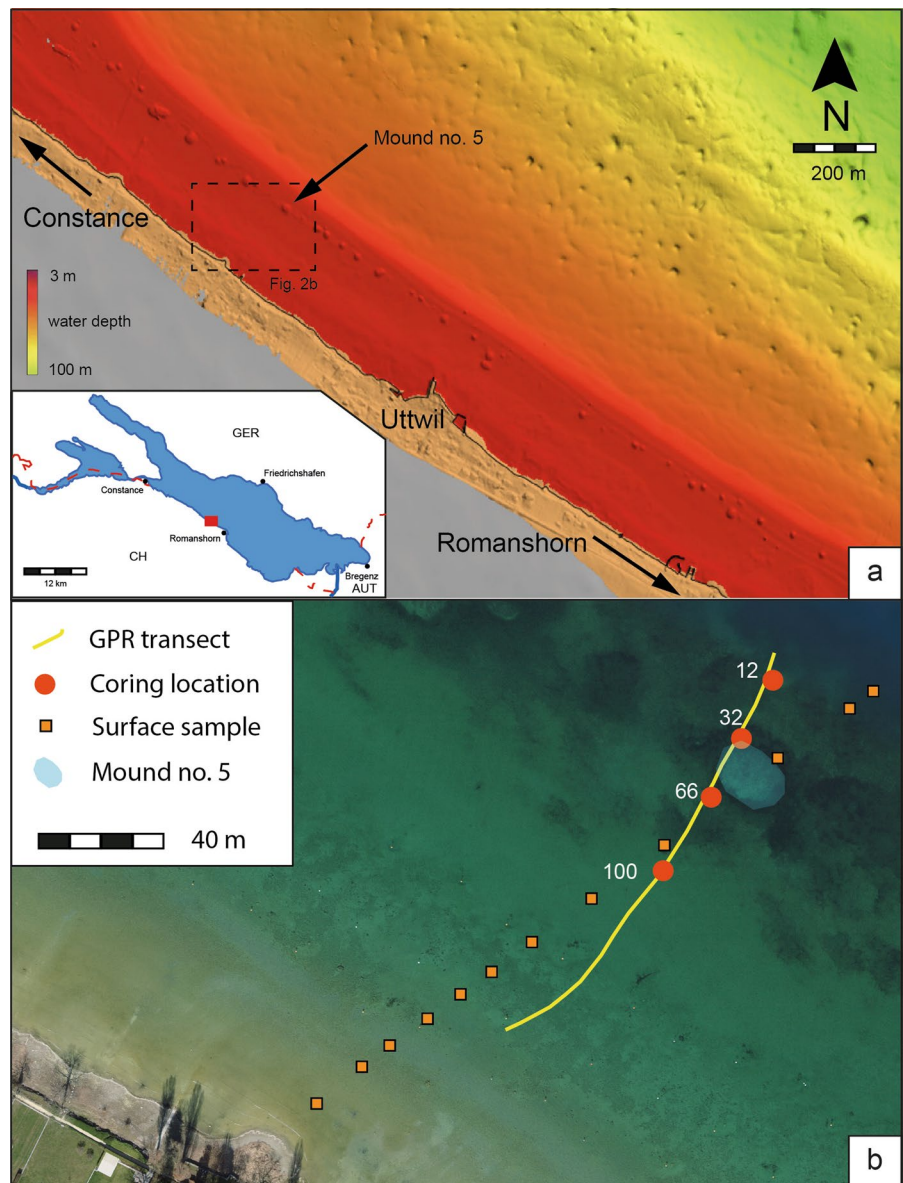


**Fig. 1** Topographic map (Swisstopo, Federal Office of Topography) showing the locations of the mounds (red dots) along the Southern Swiss shore of Lake Constance between the village of Altnau and the town of Romanshorn

be composed of more than 60 Mio individual cobbles, weighting ~78,000 t. Already upon their initial discovery, the question of a natural or anthropogenic origin of the mounds was raised (Leuzinger et al. 2021). Further geophysical, sedimentological, and archaeological investigations focused on Mound no. 5, located ~250 m offshore the village of Uttwil (Fig. 2a). An underwater ground penetrating radar (GPR) survey showed a succession of glacial till, late glacial clays and postglacial lake sediments underlying the mounds, indicating their non-glacial

and thus most likely anthropogenic origin. The survey further revealed that the mounds were initially constructed at the shelf edge and that the shelf has prograded towards the lake since then (Hornung 2018). Archaeological dives and a sampling trench in a mound retrieved multiple fragments of wood. Most of them were radiocarbon dated to 5550–5250 cal. yrs BP, suggesting that the mounds were built during the Neolithic age by local pile dwellers (Leuzinger et al. 2021). However, it is still unclear if these mounds were constructed on periodically dry land or

**Fig. 2** **a** Bathymetric map (Wessels et al. 2016) of Lake Constance showing a part of the chain of mounds along the shelf edge. **b** Orthophoto (Swisstopo, Federal Office of Topography) of the study area around Mound no. 5 showing sampling locations (surface-sediment samples and sediment cores) and the GPR transect



if they have been submerged in the lake since their construction. Calculations based on geotechnical drillings in the vicinity of the Lake Constance outlet resulted in a minimum lake level of 393 m above sea level (m a.s.l.; Swiss vertical datum), still 0.5–2.0 m above the top of the mounds (Leuzinger et al. 2021). This study presents in detail the results of a sediment-core transect carried out in 2019 across the shelf along a ground-penetrating radar line crossing a mound. The focus of this sedimentological, petrophysical and geochemical analysis is to identify changes and trends of the depositional environment reflecting the paleoenvironment before, during and after mound formation. The main aim is to reconstruct lake-level changes that may have strongly influenced relevant processes. For this purpose, the core-based paleoenvironmental reconstruction will be calibrated with modern surface samples taken at various water depths. Further, we aim to confirm the Neolithic age of the mounds by dating the sediments corresponding to the prehistoric shelf edge the mounds were constructed on.

## Site description

### Limnology

With a total surface area of 536 km<sup>2</sup>, a maximum depth of 251 m and a volume of 48.4 km<sup>3</sup>, tri-national (Germany, Austria, Switzerland) Lake Constance is one of the largest perialpine lakes. Most of the inflow (~ 65%) is brought by the Alpine Rhine River. The lake is generally divided into the larger and deeper Upper Lake (“Obersee”) and the smaller and shallower Lower Lake (“Untersee”). The mean lake level in the Upper Lake is some 395 m a.s.l. Driven by seasonal snow melt in the Alpine source area, lake-level maxima are reached in June and July. Consequently, minima occur in late winter (March) when precipitation is retained as snow. The mean annual difference between minima and maxima is 1.40 m and the observed all-time maximum difference is 3.38 m (Güde and Straile 2016). After a period of anthropogenic eutrophication during the 20<sup>th</sup> century, the lake has returned to its natural monomictic, oligotrophic state (Wessels et al. 1999; Milan et al. 2022). Sediments mainly brought in by the Rhine River are usually transported along the

northern shore (Wessels 1995; IGKB 2016). Small-scale slow currents in the shallow water areas close to the shore are mainly controlled by gradients in temperature and density while strong rip-currents are also driven by onshore winds (Wessels 1999).

### Geological setting

The greater Lake Constance area lies in the Molasse basin in the northern Alpine foreland. Most of the catchment of the Alpine Rhine River is built up by Mesozoic limestone (Helvetic nappes) and metamorphic schists (Penninic nappes) (Wessels 1998a). With the onset of the Quaternary, the Molasse substrate around Lake Constance was covered multiple times by the advancing and retreating Rhine Glacier, which led to formation of several overdeepened valleys, with the Lake Constance Basin as the largest of them. After the Last Glacial Maximum (LGM), the Rhine Glacier retreated and modern Lake Constance became ice-free (Keller 1994; Wessels 1995, 1998a, b, c).

### Previous studies of Lake Constance sediments

In general, Upper Lake Constance can be divided into three main sedimentation areas: the northern slope influenced by allochthonous clastic input from the Rhine River, the central basin characterized by turbidite deposits, and the southern slope, which is dominated by autochthonous carbonate production typical for a hard-water lake (Wessels 1995, 1998a). First sediment cores in Lake Constance were retrieved in the late 1960s near the Rhine Delta (Förstner et al. 1968). In the 1980s and 1990s, multiple coring campaigns retrieved piston cores to classify the different sediment types, map their distribution and track changes in the trophic state, lake level, and climate (Giovanoli 1991; Hofmann 1991; Ostendorp 1991; Neukirch 1991; Niessen and Sturm 1991; Niessen et al. 1992). The sediments investigated in all these campaigns cover the last ca. 17,500 cal. yrs BP and represent different depositional settings ranging from sub- to proximal glacial sediments, annually laminated loess deposits, and lake marls intercalated with flood layers (Wessels 1998b). They provided useful information about the natural change in environmental conditions and the anthropogenic influence (Kober et al. 2007; Hanisch et al. 2009;

Schwalb et al. 2013). The recovery of the longest available core, a 24 m long core from the Central Basin (Schaller et al. 2022), marks the most recent limnogeological research of Lake Constance.

### The shallow-water area

About 14% of Upper Lake Constance is part of the shallow-water area with water depths less than 10 m that mostly stretch out 200–500 m from the shore towards the lake (Güde and Straile 2016). The distribution of sediments in this ‘shelf’ area is influenced by clastic river input, autochthonous calcite precipitation and resuspension, as well as deposition by wind-induced waves (Schmieder et al. 2004; Güde and Straile 2016). Large-scale, lake-wide analyses of littoral surface sediments show a decrease in allochthonous material from east to west and north to south and decreasing mean grain sizes with increasing water depths. In general, larger mean grain sizes are observed along the northern shore (Schmieder et al. 2004; IGKB 2016). The littoral surface sediments of the southern shore are commonly described as fine- to coarse-grained without clear and distinct laminations or sedimentary structures. This is attributed to the constant redistribution and lakeward transport out of the shallow-water area (Güde et al. 2009; Güde and Straile 2016). In recent years, several studies investigated the increasing erosion of surface sediments and the resulting disintegration of archaeological artifacts of the littoral zone (Ostendorp et al. 2016; Ebersbach et al. 2019). Studies have been carried out to better understand the processes and mechanisms involved in surface-sediment distribution (Wessels and Weber 2013; Hofmann et al. 2019; Wessels and Hornung 2019).

### Archaeological background

There are few traces of Paleo- and Mesolithic human activity in the region (Leuzinger 2010). The first evidence of Neolithic pile dwellings along the Lake Constance shore dates to ca. 5900 cal. yrs BP. Throughout the Neolithic, these occupations were short-term and discontinuous. Settlements were built in multiple waves of occupation and were often abandoned and re-occupied later. With the onset of the Bronze Age (~ 4200 cal. yrs BP), the settlements became more permanent, and the Lake

Constance Area was relatively densely populated (Schlichtherle 2004; Billamboz 2014; Benguerel et al. 2020). The first written sources of human activity in the region date to the time of Roman occupation (~ 2000–1600 cal. yrs BP). Alamannic settlement along the Northern and Southern shores of Upper Lake Constance occurred from ~ 1750 to 1250 cal. yrs BP (Leuzinger 2013). Well-preserved sites from the Neolithic and Bronze Age are found especially along the German shores of the Lower Lake (e.g., Hornstaad Hörnle) and the Überlingen Basin of the Upper Lake (e.g., Sipplingen, Bodman, Unteruhldingen) (Kolb 1997; Köninger 1997; Dieckmann et al. 1997). On Swiss territory, three of the most intensely studied areas are those of Upper Lake (Arbon-Bleiche 2 and 3), Lower Lake (e.g., Steckborn, Ermatingen, Eschenz) and Seebachtal (Nussbaumersee, Ürschhausen-Horn), ~ 40 km to the west (Hasenfratz 1997; Jacomet et al. 2004; Brem and Leuzinger 2016). However, up to today, there is no direct evidence for settlements in the vicinity of mound no. 5 around ~ 5450 BP (Leuzinger et al. 2021). Since 2011, a total of 111 representative sites from France, Italy, Switzerland, Germany, Austria, and Slovenia are listed as UNESCO-World Heritage Site *Prehistoric pile dwellings around the Alps*. Eleven of those selected sites are found along the shores of Lake Constance (Hagmann and Schlichtherle 2011).

## Materials and methods

### Geophysical methods

The underwater GPR survey was performed in April 2018 offshore the settlements of Uttwil, Romanshorn and Güttingen. Multiple profiles running parallel and orthogonal to the shoreline in the vicinity of eight different mounds were recorded with a bistatic broadband antenna (Geophysical Survey Systems Inc.) at 200 MHz frequency, which was drawn directly above the sediment surface. The antenna was towed along the transect at a measurement interval of 0.7–1.0 cm in a water-tight casing on a sled developed at TU Darmstadt (Hornung 2023). The data were processed with the software ReflexW (Sandmeier Scientific Software), travel times were converted to

depth by using a wave velocity of 0.05 m/ns for all profiles (Hornung 2018).

### Sediment coring and surface-sediment sampling

A coring campaign was carried out in June 2019. The four coring sites are located along a GPR transect in the shallow-water area on the southern shelf (Hornung 2018, Fig. 2b). Coring was performed from an anchored inflatable coring platform in a water depth of 3.4–4.7 m. A percussion piston-coring system was used with a barrel length of 3 m and a diameter of 6 cm. For each coring location, a gravity short core and one to two piston cores were taken with an overlap of ~ 50 cm. Cores were cut into ~ 1-m long sections for better handling. In total, 11 cores were retrieved and cut into 25 sections. The sections were labelled after the coring locations and core number (e.g., BO\_32\_3A is the first section (A) from the 3<sup>rd</sup> core (3) of coring site BO\_32). The sediment-surface samples were taken by archaeological divers from the AATG in May 2020. Twelve samples were recovered along a water-depth transect from 0.5 to 6.0 m. This transect also follows the GPR transect (Fig. 2b).

### Sediment description and analysis

Core sections were analyzed for wet bulk density (WBD) and magnetic susceptibility (MS) at 5 mm resolution with a GEOTEK-multi-sensor-core-logger (MSCL). The two lowermost sections (BO19\_100\_3B and BO19\_100\_3C) were additionally analyzed with X-ray computed tomography (CT) at the Institute of Forensic Medicine, University of Bern. Afterward, the cores were split in half, photographed (Geotek linescan) and macro- and microscopically described (texture, colour, sedimentological structures). For the microscopical description of the texture, smear slides were produced. Samples for geochemical laboratory analyses were taken every 20 cm, freeze-dried, and then powdered and homogenized with pestle and mortar. Total carbon (TC), nitrogen (TN) and sulphur (TS) measurements were performed on a CHNS elemental analyser (Thermo Scientific Flash 2000). Total inorganic carbon (TIC) was measured with a multi-element EA 2000CS. Total organic carbon (TOC) content was calculated by subtracting TIC from TC. The carbonate content in weight percent (wt% CaCO<sub>3</sub>) was calculated by

multiplying TIC by 8.33. Organic matter content (wt% OM) was calculated by multiplying TOC by 1.8 (Meyers and Teranes 2001). Fourier transform infrared spectroscopy (FTIRS) was used to measure the biogenic silica content (wt% bSi) following the method described by Meyer-Jacob et al. (2014) using a Bruker Vertex 70 HTS-XT instrument set up and sample preparation as described in Vogel et al. (2016). Siliciclastic wt% (SiIC) was calculated by subtracting CaCO<sub>3</sub>, OM and bSi wt% from 100%. Volumetric (vol%) particle-size distribution (PSD) was measured by laser-diffraction analysis (LDA). To break up naturally formed aggregates, organic matter was dissolved with 30% hydrogen peroxide (H<sub>2</sub>O<sub>2</sub>). The samples were then further dispersed by adding a dispersion solution consisting of a mixture of sodium hexametaphosphate (NaPO<sub>3</sub>) and sodium carbonate (Na<sub>2</sub>CO<sub>3</sub>) and shaking them overnight (Ryzak and Bieganski 2011). In addition, aggregate-forming carbonates were dissolved with 5% hydrochloric acid (HCl) (Murray 2002). Measurements were carried out on a Malvern Mastersizer 2000 at the Institute of Geography of the University of Bern. Measurements for TIC, TC, TN, TS (CNS), bSi (FTIRS) and PSD-LDA as well as the calculations of CaCO<sub>3</sub>, OM, bSi and SiIC were carried out on the surface samples in the same way as for the core samples.

### Composite profile

Based on macroscopic sedimentological structures (e.g., distinct layers) and MSCL data, overlapping sections between piston cores were correlated to establish a composite section for each coring location. These composite profiles of all four cores were then visually correlated along prominent layers guided by the GPR stratigraphy and the radiocarbon ages resulting in a 12.4-m long dual composite section (hereafter termed composite<sup>2</sup> section, or simply BO19). The two correlations between cores BO19\_12 and BO19\_32 and between cores BO19\_32 and BO19\_66 pose some uncertainties as no clear and distinct layers could be identified. The depth scale used for the composite<sup>2</sup> depths refers to cm composite depth (cmcd).

Age-depth model

Core sediments were sieved for organic remains usable for accelerator mass spectrometer radiocarbon dating (AMS <sup>14</sup>C). In total, 13 samples of small, terrestrial fragments were measured at the Laboratory for the Analysis of Radiocarbon with AMS (LARA), University of Bern (Szidat et al. 2014) (Tab. 1).

The radiocarbon ages were calibrated by using the IntCal20 calibration curve (Reimer et al. 2020) within the software Bacon v2.5.8 (Blaauw and Christen 2011). The software was also used to create an age model for the composite<sup>2</sup> section. In this manuscript, we refer to the weighted mean age rounded to decades when providing ages and age ranges.

**Table 1** Accelerator mass spectrometer radiocarbon age determinations

Lab code	Core section	Composite depth [cm]	Composite <sup>2</sup> depth [cm]	Radiocarbon age [yrs BP ± 1σ]	Calibrated age [yrs BP, 2σ]	Remarks
BE-16962.1.1	12_2A	123	123	3078 ± 68	3447–3077	gas measurement
BE-16963.1.1	12_2B	221	221	3634 ± 69	4151–3724	gas measurement
BE-16964.1.1	12_2C	321	321	4222 ± 89	5026–4449	gas measurement
BE-11676.1.1	32_2C	226	425	4788 ± 38	5594–5335	graphite measurement
BE-16965.1.1	32_3A	342	541	7061 ± 148	8176–7618	probably reworked material
BE-16966.1.1	32_3B	442	641	6552 ± 89	7582–7278	gas measurement
BE-16967.1.1	32_3C	542	741	7565 ± 119	8599–8040	gas measurement
BE-16968.1.1	66_3A	367	898	11,117 ± 112	13,231–12,767	gas measurement
BE-16969.1.1	66_3B	456	987	12,093 ± 165	14,829–13,528	gas measurement
BE-16970.1.1	66_3C	495	1026	12,202 ± 185	14,988–13,617	gas measurement
BE-16971.1.1	100_2C	304	1016	–	–	measurement not reliable
BE-16972.1.1	100_3B	339	1051	12,223 ± 306	15,290–13503	gas measurement

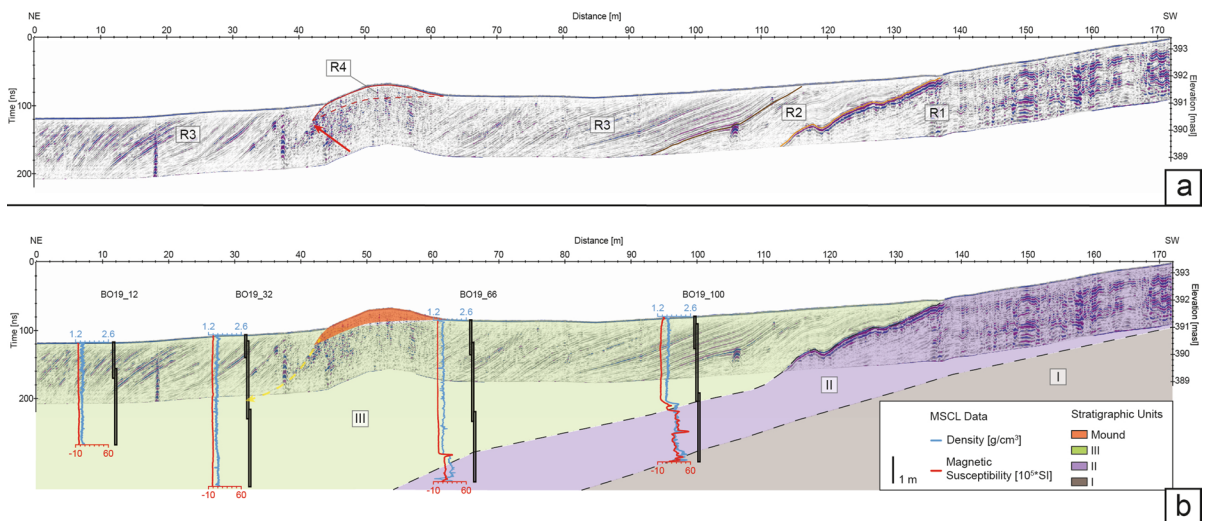


**Fig. 3** a GPR line (Hornung 2018) across mound no. 5 with four radar facies R1-R4 (boundaries marked by coloured lines) and prehistoric shelf edge (red arrow) b compilation of the GPR line with sediment-core locations, stratigraphic units

and MSCL data (MS and WBD). Correlation between the prehistoric shelf edge and the cores is indicated by the yellow arrow

Description	Line Scan	Description	Line Scan
<p><b>Lithotype A</b> <span style="color: yellow;">■</span></p> <p>silty fine sand, beige-brown shell fragments, plant remains massive, homogeneous on top of every short core</p> <p>WBD: 1.1 - 1.7    MS: -5.4 - 4.4 CaCO<sub>3</sub>: ~67    SiC: ~30 OM: ~2    bSi: ~1</p>	<p>66_KK1</p>	<p><b>Lithotype B</b> <span style="color: green;">■</span></p> <p>finesandy, clayey silt beige-grey-brown no-multiple shells/fragments laminations of few cm thickness found in each composite core</p> <p>WBD: 1.3 - 1.8    MS: -4.6 - 6.7 CaCO<sub>3</sub>: 54 - 87    SiC: 11 - 45 OM: 1 - 3    bSi: &gt;2</p>	<p>32_2C</p>
<p><b>Lithotype C</b> <span style="color: darkgreen;">■</span></p> <p>finesandy, clayey silt beige-grey-brown no-multiple shells/fragments laminations of few mm thickness found in composite cores 12, 32, 66</p> <p>WBD: 1.3 - 1.8    MS: -4.3 - 2.0 CaCO<sub>3</sub>: 55 - 87    SiC: 11 - 43 OM: 1 - 3    bSi: &gt;2</p>	<p>32_2B</p>	<p><b>Lithotype D</b> <span style="color: cyan;">■</span></p> <p>finesandy, clayey silt beige-grey few shells/fragments massive, homogeneous found in composite cores 12, 32, 66</p> <p>WBD: 1.4 - 1.6    MS: -4.4 - -1.0 CaCO<sub>3</sub>: 61 - 84    SiC: 13 - 36 OM: &gt;2    bSi: &gt;2</p>	<p>32_2B</p>
<p><b>Lithotype E</b> <span style="color: magenta;">■</span></p> <p>clayey silt, grey-black no shells/fragments laminations of few mm thickness found in composite cores 66, 100</p> <p>WBD: 1.6 - 1.8    MS: 1.1 - 29.8</p>	<p>66_3C</p>	<p><b>Lithotype F</b> <span style="color: darkblue;">■</span></p> <p>clayey silt, few fine gravel, grey no shells/fragments massive, homogeneous found in composite cores 66, 100</p> <p>WBD: 1.7 - 2.0    MS: 4.0 - 36.3 CaCO<sub>3</sub>: ~26    SiC: ~72 OM: &lt;1    bSi: ~1</p>	<p>66_3C</p>
<p><b>Lithotype G</b> <span style="color: orange;">■</span></p> <p>silty, clayey fine-coarse sand brown-beige-grey no shells/fragments alternations of finer and coarser layers found in composite core 100</p> <p>WBD: 1.3 - 2.1    MS: 8.9 - 19.3 CaCO<sub>3</sub>: ~41    SiC: ~58 OM: &gt;1    bSi: &gt;1</p>	<p>100_A</p>	<p><b>Lithotype H</b> <span style="color: brown;">■</span></p> <p>clayey silt to silty clay beige/yellowish-brown scattered middle-coarse gravel laminations of multiple cm thick- ness found in composite cores 66,100</p> <p>WBD: 1.8 - 2.2    MS: 13.2 - 56.5 CaCO<sub>3</sub>: ~28    SiC: ~71 OM: &gt;1    bSi: &gt;1</p>	<p>100_3C</p>
<p><b>Lithotype I</b> <span style="color: brown;">■</span></p> <p>clayey silt to silty clay beige/yellowish-brown scattered middle-coarse gravel disturbed lamination/patches of different color found in composite cores 66, 100</p> <p>WBD: 1.2 - 2.1    MS: 8.6 - 35.3 CaCO<sub>3</sub>: ~28    SiC: ~71 OM: &gt;1    bSi: &gt;1</p>	<p>66_3C</p>	<p><b>Lithotype J</b> <span style="color: grey;">■</span></p> <p>clayey silt to silty clay beige-brown abundant medium-coarse gravel massive, homogeneous found in composite core 100</p> <p>WBD: 1.9 - 2.4    MS: 14.8 - 44.4 CaCO<sub>3</sub>: 27 - 36    SiC: 63 - 71 OM: &gt;1    bSi: ~1</p>	<p>100_3C</p>



◀**Fig. 4** Summary of the lithotypes including macroscopic sedimentological description, geochemical and petrophysical properties, Geotek linescan and lithotype code used in Figs. 7 and 8. *WBD* wet bulk density [ $\text{g}/\text{cm}^3$ ], *MS* magnetic susceptibility [ $\text{SI} \cdot 10^{-5}$ ], *CaCO<sub>3</sub>* carbonate [wt%], *SilC* siliciclastic [wt%], *OM* organic matter [wt%], *bSi* biogenic silica [wt%]

## Results

### GPR stratigraphy

The GPR line (Fig. 3a) images in detail the stratigraphic architecture of the shallow-water zone down to a sediment depth of ~ 2–3 m. Based on the geometrical properties (e.g., shape, thickness, continuity, and inclination) of the reflections, four radar facies (R1–4) were distinguished; R1 (oldest) to R3 (youngest) form a conformable stratigraphic succession representing three distinct periods. R4 is a locally confined radar facies that is embedded within R3 (Hornung 2018): R1 shows a continuous, high-amplitude reflection at the top with a sharp boundary to the overlying facies and very little further signal penetration. R2 is characterized by continuous, parallel inclined low-amplitude reflections with intercalated discontinuous, chaotic very low-amplitude reflections and diffraction hyperbolas. R3 initially shows continuous parallel high- to medium-amplitude reflections, which are generally inclined towards the lake forming clinofolds. Subsequent clinofolds are intercalated with low-amplitude, discontinuous, and wavy to chaotic reflections. Both sub-types of R3 show repetitive patterns of high to low amplitudes forming distinct reflection packages repeating in hierarchical patterns showing larger-scale trends. The inclination of clinofolds increases towards the lake basin and their shape converts from concave to convex. R4 shows a rather chaotic facies; it is formed by the mound itself and is defined by overlapping, hyperbolic high-amplitude reflections that are interpreted to be caused by the individual rocky blocks in an unmigrated GPR section (diffraction hyperbolas). Some high-amplitude reflections (single blocks) continue in an inclined, lakeward direction. The GPR line clearly documents that the mound (R4) is embedded within R3 indicating that it is not connected to the R2 or R1 units below (Fig. 3a).

### Core sedimentology and stratigraphy

Based on macro- and microscopic sedimentological description and petrophysical and geochemical analysis, the core lithologies were grouped into ten lithotypes. Fig. 4 provides detailed information of all lithotypes with characteristic core photographs as well as their sedimentological, petrophysical and geochemical signatures. In addition, the lowermost two sections of the composite core are shown in Fig. 5 including their CT images. The succession of lithotypes is further divided into three stratigraphic units I–III (Fig. 3b). Figure 6 displays the succession of the stratigraphic units as part of the composite<sup>2</sup> section with the composite depth profiles of wet bulk density, magnetic susceptibility, sediment composition, PSD and AMS <sup>14</sup>C measurements. Unit I (Lithotype J, 1203.9–1243.9 cmcd) is built up by beige to brown, homogeneous clayey silt to silty clay with medium- to coarse-sized gravel forming a matrix-supported diamictic fabric (Fig. 5). Unit I shows low content in carbonate (27–36 wt%) and high content in siliciclastic (63–71 wt%). Unit I is also characterized by high magnetic susceptibility (up to  $44.4 \text{ SI} \cdot 10^{-5}$ ) and the highest density ( $1.9\text{--}2.4 \text{ g}/\text{cm}^3$ ). Stratigraphic Unit I was only recovered in coring site BO19\_100. Unit II (lithotypes E–I, 1023.3–1203.9 cmcd) shows a succession of grey, partially black-spotted, finely laminated to homogeneous clayey silt (lithotypes E and F), a silty, clayey sand layer (Lithotype G), and beige to yellowish and brown, laminated silt and clay with scattered gravel clasts (lithotypes H and I). Similar to Unit I, Unit II shows low contents of carbonate and high contents of siliciclastic. The magnetic susceptibility falls in the same range as in Unit I, wet bulk density is slightly decreased ( $1.2\text{--}2.2 \text{ g}/\text{cm}^3$ ). Unit II was recovered in coring sites BO19\_66 and BO19\_100 with the exception that Lithotype G (silty, clayey sand) only occurs in two sections of coring site BO19\_100. Unit III (lithotypes A–D, 0–1023.3 cmcd) consists of beige, grey and brown, fine-sandy to clayey silt with a cap of silty fine sand (Lithotype A) on top. The silt appears either laminated (lithotypes B and C) or homogeneous (Lithotype D). Snail shells appear throughout the whole succession. Unit III is characterized by the lowest wet bulk density ( $1.1\text{--}1.8 \text{ g}/\text{cm}^3$ ) and magnetic susceptibility ( $-5$  to  $7 \cdot 10^{-5}$ ) values and the highest carbonate content (54–87 wt%). Unit III

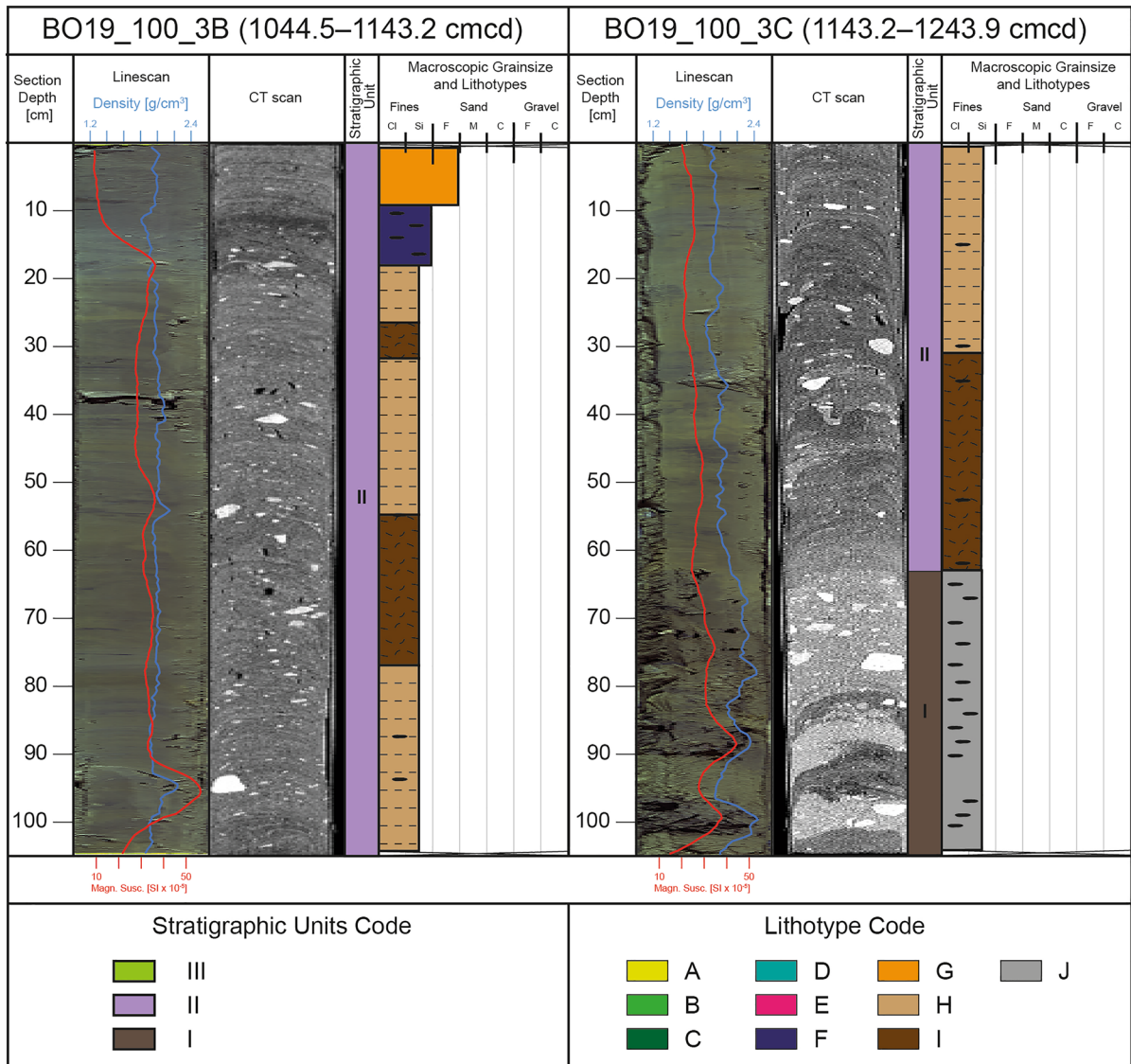


**Fig. 5** Compilation of Geotek linescan, CT scan and lithotypes for sections BO19\_100\_3B (left) and BO19\_100\_3C (right)

was recovered at every coring site. From ~ 950 to 900 cmcd (~ 13,400–12,820 cal. yrs BP), a first decrease of carbonate content (down to ~ 55 wt%) is observed. An upcore trend of decreasing carbonate content then occurs starting from ~ 750 cmcd (~ 9010 cal. yrs BP) to a plateau of minimum values of ~ 55 wt% at ~ 450–350 cmcd (~5750–4950 cal. yrs BP), which is overlain by a subsequent rise until the top of the core. The siliciclastic content in- and decreases inversely proportional to the carbonate content. For the same interval, we also observe a respective decrease,

plateau, and subsequent increase in the contents of the clay and fine silt grain fractions. This is also expressed by in- and decreasing mean and median grain sizes.

Surface-sediment samples

The results of the geochemical (CNS, FTIRS) and PSD-LDA analysis performed on the surface samples are plotted against their respective water depth (Fig. 7). The PSD shows the highest proportions of

sand (45–90 vol%) in a water depth of 0.5–1.5 m below which a drop to the lowest values (< 10 vol%) occurs. The proportion of sand then peaks again at 3.0 m water depth with 60 vol% and decreases steadily towards 20 vol% at 5.0 m water depth. A subsequent rise towards 50% is observed from 5.0 to 6.0 m water depth. In general, a trend of decreasing mean and median grain size with increasing water depth can be deduced. Carbonate content generally increases with increasing water depth: it rises from ~ 30–50 wt% in a water depth < 3 m towards contents of 50–65 wt% in water depths of 3–6 m. The siliciclastic content inversely decreases with increasing water depth.

### Age model

Results of the AMS  $^{14}\text{C}$  measurements, calibrated ages and composite depths of the samples are provided in Table 1. From the 13 analyzed samples, one measurement (BE-16971.1.1) was not measurable. Another sample (BE-16965.1.1) did not follow the general age-depth trend and was interpreted as reworked material and therefore excluded from the age model. The remaining samples lie in the age range from ~ 14,390 to 3270 cal. yrs BP, i.e., from the late glacial throughout most of the Holocene. The age model (Fig. 8) covers the sedimentary succession of Unit III and ranges from ~ 14,440 to 1960 cal. yrs BP. Coring site BO19\_32 was specifically selected to cover the sediments corresponding to the prehistoric shelf edge the mound was constructed on. The GPR reflection corresponding to the prehistoric shelf edge was extrapolated to the coring site (Fig. 3). Using this approach, the sediments deposited during mound construction are expected at ~ 425 cmcd. Using this approach, Mound no. 5 was dated to ~ 5520 cal. yrs BP (sample BE-11676.1.1), coinciding with radiocarbon dated wood that was excavated directly in the mounds (Leuzinger et al. 2021).

## Discussion

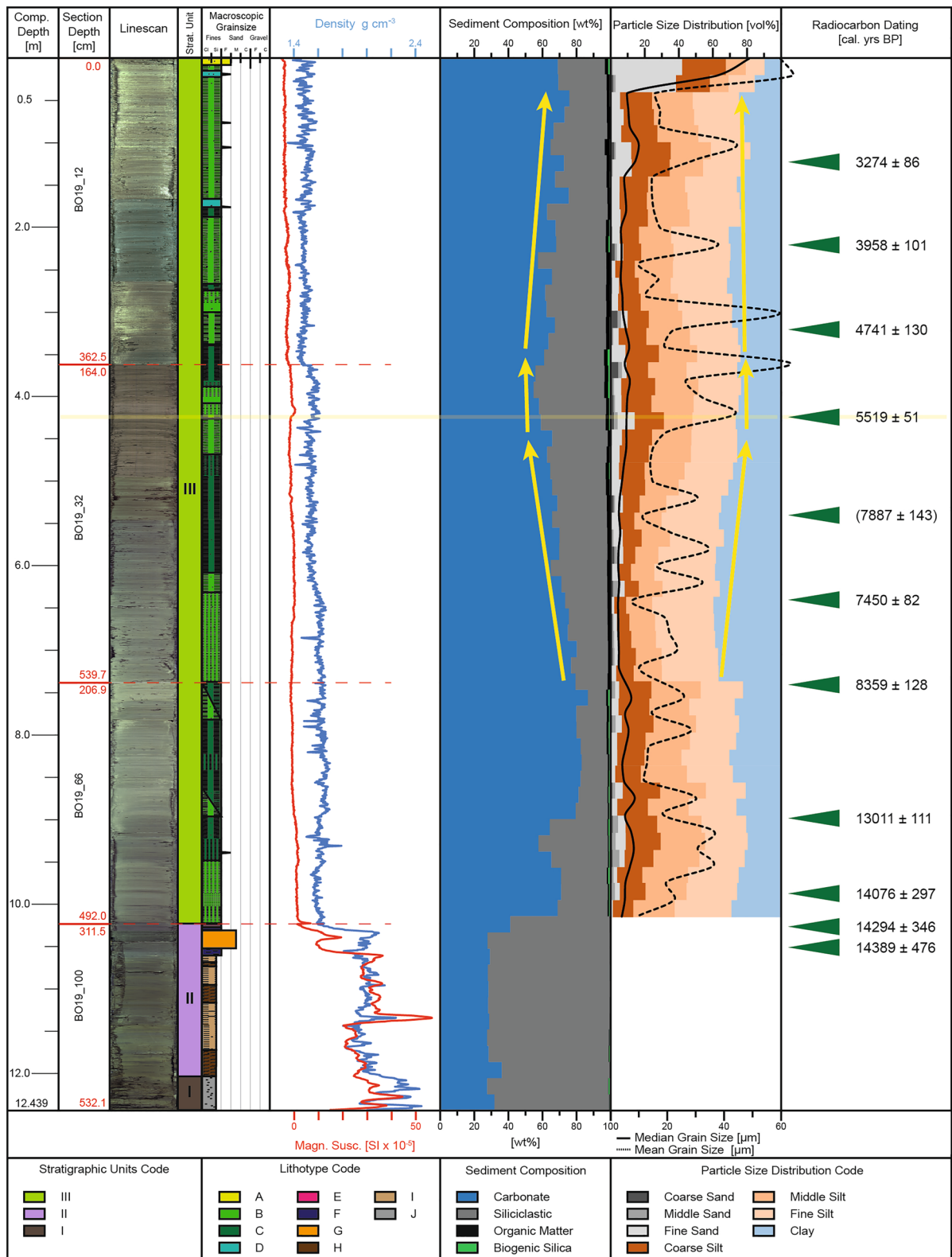
### Core-to-GPR correlation

The three radar facies R1–R3 identified by GPR are correlated to the sedimentological record of the cores (Fig. 3b). Facies R4, representing the mound, was not recovered in the cores, as the applied coring device

is not able to penetrate boulders. The boundary between R3 and R2 could not be correlated to a lithologic change in the composite core BO19\_100. There is neither a distinct sedimentological layer nor a noticeable change in the petrophysical data so that radar facies R3 and R2 together are correlated to stratigraphic Unit III. Due to limited radar penetration, the boundary between R2 and R1 cannot be traced from the shore- proximal area to coring site BO19\_100 closest to the shore (Fig. 3). However, extrapolating the prominent reflection clearly suggests its occurrence in composite cores BO19\_100 and BO19\_66 coinciding with the prominent changes in lithology and petrophysical data at the Unit II–III boundary (Fig. 3). Therefore, we attribute R1 to stratigraphic Unit II. Unit I is only recovered in composite core BO19\_100 at a depth of ~ 4.9 m. Due to the maximum penetration depth of the GPR of ~ 2–3 m, Unit I was not identified in the GPR campaign.

### Interpretation of GPR data and core lithologies: depositional evolution of the shelf area

The matrix-supported diamictic fabric of the lowermost stratigraphic Unit I is interpreted as till deposited during the last glaciation. It correlates to the basal lodgement till that covers extensive areas of the hills south of Lake Constance (Zaugg et al. 2008). The top of a gravel-rich bed visible in the CT scan (Fig. 5) marks the boundary to overlying stratigraphic Unit II comprised of more finely laminated sediments. Scattered, individual gravel clasts coincide with peaks in wet bulk density and magnetic susceptibility. The change from Unit I to Unit II is interpreted as the final retreat of the Rhine Glacier from the Lake Constance area after a short readvance (“Stein am Rhein” stage) after 20,600 cal. yrs BP (Kamleitner et al. 2023). Afterwards, a cold proglacial lake dominated by clastic sedimentation formed and led to deposition of Unit II. Individual clasts are interpreted to represent dropstones, i.e., glacial debris from floating icebergs, indicating that the glacial front still was in contact with Lake Constance. Unit II thus represents the clastic pro- and postglacial sedimentation (Wessels 1998c). The change to the carbonate-rich sediments of Unit III documents the transition towards a more temperate lake and onset of biologic productivity, resulting in the deposition



◀**Fig. 6** Log sheet of the composite<sup>2</sup> section BO19. Yellow arrows indicate general trends in carbonate content and particle-size distribution. The sediment horizon that was correlated to the prehistoric shelf edge of mound construction is highlighted by the yellow bar

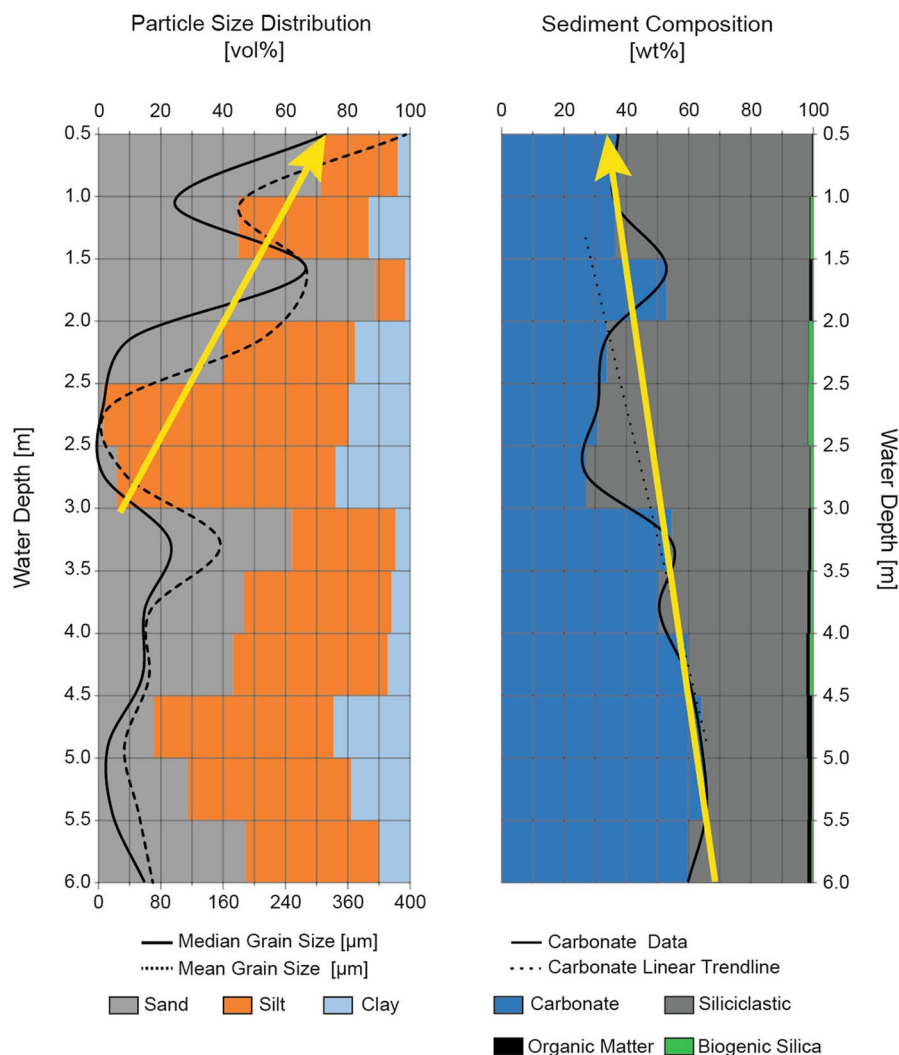
of endogenic lacustrine chalk (Wessels 1998c). The continuous, parallel reflections recognized in the GPR data represent regular deposition in periods of calm weather, whereas intercalated, chaotic reflections are interpreted as storm deposits (tempestites). Repeated reflection packages indicating low-energy sediments at their base and terminating in tempestites point to pronounced short-term climate fluctuations superpositioned on long-term trends. These mixed clastic-endogenic lake deposits create a prograding shelf-edge system. Controlled by wave-base remobilization and currents, the laterally stacked clinofolds identified by GPR indicate that the shelf edge prograded from a shore-proximal location over 100 m out into the lake. GPR data and sediment cores clearly show that the mounds are separated from the glaciolacustrine deposits (Unit II) as they are deposited on top of the laterally prograding lacustrine shelf deposits (Unit I; Fig. 3b). This excludes the mounds to be a natural relict of buried elongated till such as a side moraine, clearly pointing towards an anthropogenic origin. The prehistoric shelf edge coinciding with the mounds is marked by radar reflections with exceptionally high amplitudes (arrow in Fig. 3a). They are likely caused by rocks rolling down the edge during mound construction or destruction, confirming the assumption that the mound was constructed at the shelf edge at that time. Radiocarbon dating of the uppermost layers of Unit II and the lowermost layers of Unit III shows that proglacial clastic sedimentation lasted at least until ~ 14,400 cal. yrs BP and ceased latest at ca. 14,000 cal. yrs BP. This age range suggests that calcite precipitation started with the end of the Oldest Dryas and onset of the Bølling-Allerød (Clark et al. 2012). The short interval of lower carbonate content from 950 to 900 cmcd (~ 13,400–12,820 cal. yrs BP) is interpreted as drop in productivity due to changing climate conditions, which coincides, within the uncertainties of the age model, with the Younger Dryas cold period (~ 12,900–11,700 cal. yrs BP)

(Clark et al. 2012). This signal is also reported from other cores recovered from the deeper part of Lake Constance (Schaller et al. 2022).

#### Lake-level changes and implications for mound construction

Since the deglaciation, the lake level of Lower Lake Constance is limited by the height of multiple alluvial fans deposited in the narrow strait between the villages of Öhningen (Germany) and Eschenz (Switzerland) (Müller 2011) and the outlet of Upper Lake Constance at the city of Konstanz. The lowest possible level of Lake Constance as defined by the minimal elevation of the underlying moraine in the outflow area and a minimal depth of the outflowing Rhine amounts to 392.5 m a.s.l. (Leuzinger et al. 2021), which is still ~ 1 m above the crest of mound no. 5. Periods of higher lake levels are commonly associated with higher annual precipitation, colder summer temperatures and a reduced seasonal vegetation period. Times of lower lake levels, in contrast, are interpreted as periods of low precipitation and rather warm temperatures (Müller 2011). Using a series of prehistoric morphologic and archaeological lake-level markers (i.e., palaeo beach terraces and cultural layers), a general decreasing lake level from 400 to 401 m a.s.l. at 9000–8000 cal. yrs BP towards 392–394 m a.s.l. at 5000–3700 cal. yrs BP is inferred. Afterwards, the lake level is interpreted to increase gradually to a maximum elevation of 397 m a.s.l. during the Roman period (Müller 2011; Vogt 2020). This general lake-level reconstruction can now be compared with sediment-core and surface-sediment data: the modern calibration obtained by the surface sediments indicate (i) a slight increase in carbonate content and (ii) a decrease in grain size with increasing water depth (Fig. 7). Applying these trends to the composite<sup>2</sup> section above 750 cmcd (Fig. 6) indicates a trend to decreasing and subsequent increasing water depth, with a mid-Holocene low stand from ~ 350–450 cmcd (~ 5750–4950 cal. yrs BP) which coincides with the extrapolated prehistoric shelf edge at 425 cmcd (~ 5520 cal. yrs BP). In combination with radiocarbon dating of the wooden piles found on the mound (5550–5250 cal. yrs BP; Leuzinger et al. 2021), it is interpreted

**Fig. 7** Particle-size distribution (left) and sediment composition (right) analysis of surface-sediment samples. Yellow arrows indicate general trends



that the mounds were constructed during a period of low lake levels when the shoreline was closer to the lineament of the mounds as it is today. However, the trends inferred from the modern surface-samples transect are not fully unambiguous and may not be representative for the whole area along the chain of mounds. Besides the water depth, other factors like temperature or small-scale current-related processes probably control the grain size and carbonate content in the shallow-water area. In addition, the gradual decline in carbonate content measured from 720 to 400 cmcd ( $\sim 8520$ – $5330$  cal. yrs BP) is also reported from other Lake Constance sediment studies and is linked to the filling of lakes in the upstream Rhine Valley that acted as sediment traps (Wessels 1998b).

This led to an increased supply of allochthonous sediment into Lake Constance and might cause part of the observed decreasing carbonate concentrations. Besides, the initial shallowing inferred from the composite<sup>2</sup> core can be related to the aggrading nature of sedimentation. Furthermore, multiproxy records report a global, centennial scale climatic change occurring at  $\sim 5600$ – $5000$  cal. yrs BP in west-central Europe that is expressed in general colder and wetter climate and referred to as the onset of the Neoglaciation period or the mid-Holocene climatic reversal (Magny and Haas 2004; Magny et al. 2006). Lake-level data from the Jura Mountains, the Swiss Plateau and the French Alps document a phase of higher lake level at  $5650$ – $5200$  cal. yrs BP

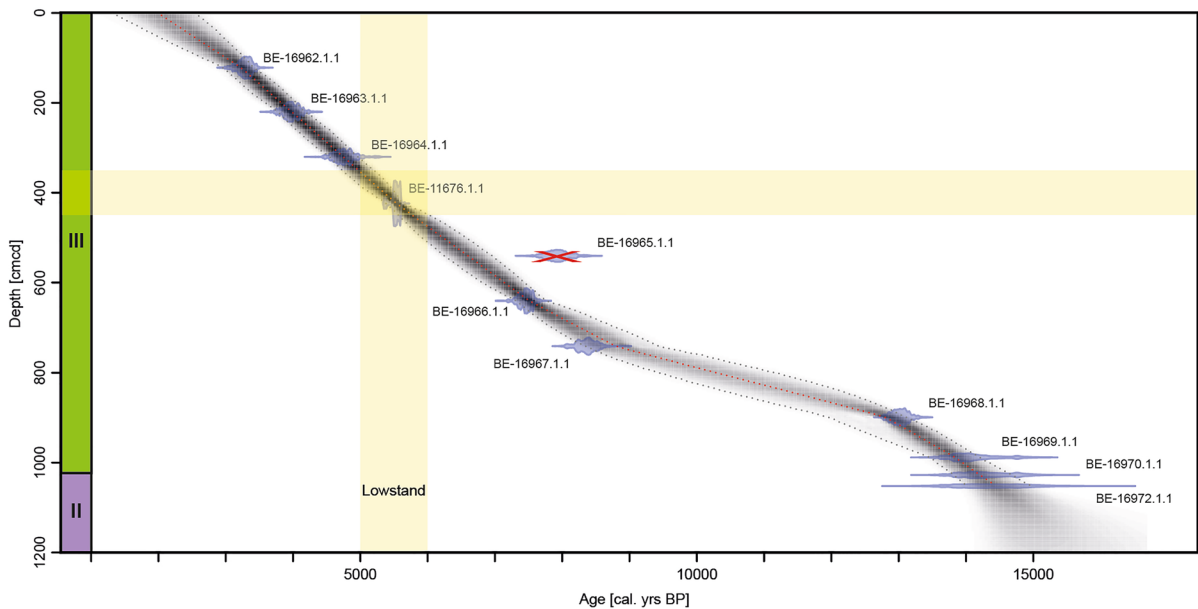


**Fig. 8** Age-depth model of the postglacial lacustrine section of the composite<sup>2</sup> core BO19 using IntCal20 and a Bacon model (Blaauw and Christen 2011; Reimer et al. 2020). The

model shows the calibrated <sup>14</sup>C ages (blue), 95% confidence interval (grey) and best model based on the weighted mean age of each depth (red)

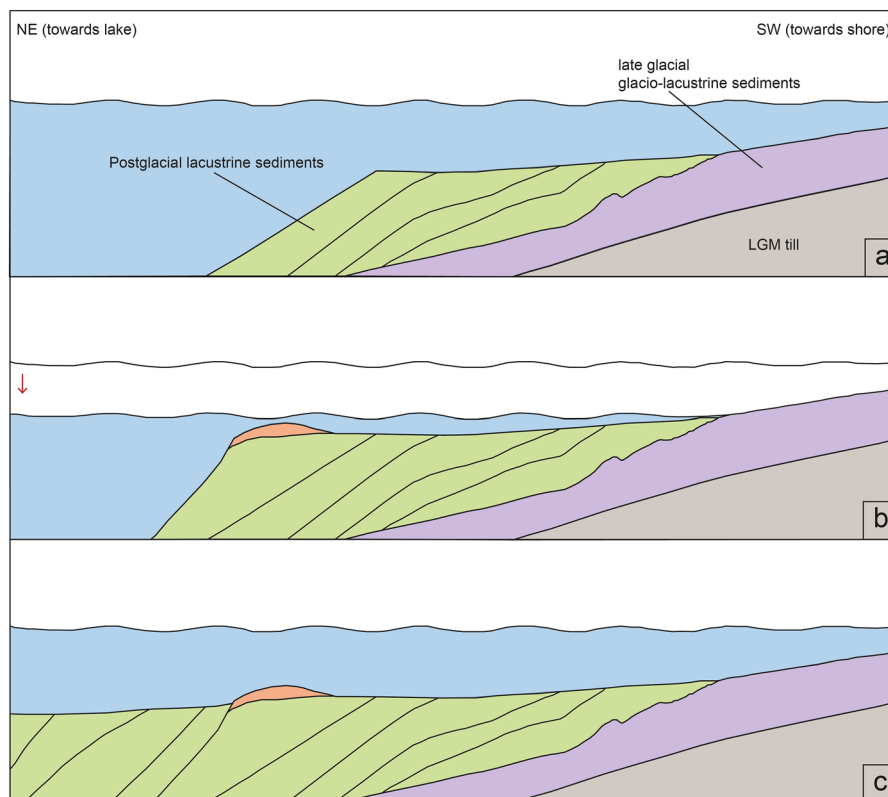
(Magny 2004, 2007). On the other hand, the water-depth increase inferred from the upper part of the composite<sup>2</sup> core is significant, as it works against ongoing accumulation. Besides, the GPR data show a change in the geometry of the reflections in stratigraphic Unit III (lacustrine chalk): from flat line reflections in the late-/postglacial they develop into a more concave shape in the first half of the Holocene. Around the horizon of mound construction, another change towards planar and finally convex reflections occurs. This change in reflection geometry implies a shift in coastal morphology, currents or water depth that are possibly related to a lowering of the lake level. Moreover, at the archaeological site of Arbon-Bleiche 3, ~ 12 km southwest of the study area, cultural layers were deposited at an exceptional lake level low stand at 5334–5320 cal. yrs BP (Jacomet et al. 2004; Magny et al. 2006), which was followed by a sudden rise that contributed to the abandonment of the settlement. In general, cultural layers and other archaeological findings along the southern shore of Lake Constance from the time of mound construction (i.e., the change from *Pfyn-* to *Horgen-*culture) are rare. This could be explained by subsequent erosion due to a rapid lake-level rise. We therefore propose

that the mounds were deposited during a short scale interval of lowered lake level following a phase of higher lake level at 5600–5500 cal. yrs BP and before a transgression starting at 5320 cal. yrs BP (Fig. 9).

## Conclusions

The southern shelf of Lake Constance holds one of the largest Neolithic structures in Europe composed of ~ 170 submerged mounds aligned over a distance of 10 km in water depths of 3–5 m. Combining data from ground penetrating radar and from a transect of sediment cores shows that the mounds were formed on a prograding shelf composed of Holocene mixed clastic-endogenic lake sediments that overlie late glacial siliciclastic sediments and glacial till. Unlike previously speculated, the mounds are thus not part of a natural elevated ridge, such as a side moraine of the Rhine Glacier, but are of anthropogenic origin. The Holocene lake sediments form a wave-base and current-controlled prograding shelf system with the mounds being constructed at the prehistoric shelf edge. Radiocarbon dating of the cored sediments corresponding to the prehistoric shelf edge suggests

**Fig. 9** Schematic evolution of the Lake Constance shelf area **a** before, **b** during, **c** after mound construction



a Neolithic age (5600–5300 cal. yrs BP) for the time of mound formation. This is in accordance with ages inferred from wood fragments from one of the mounds. Based on a water-depth calibration of carbonate content and grain size from recent surface samples in combination with findings from nearby archaeological sites, we conclude that the mounds probably were constructed during a rather short interval of relatively low lake level during a phase of climatic cooling that was followed by a transgression. Ultimately, the geophysical, sedimentological and geochemical data, combined with the morphology-based lowest-possible lake level, indicate that the mounds were at least partially submerged during their construction.

**Acknowledgements** We thank Stefano Fabbri and Valentin Nigg for help during the coring campaign. Nicole Schwendener from the Institute of Forensic Medicine, University of Bern is acknowledged for performing the CT scans. We thank Julijana Gajic from the Institute of Geological Sciences (UniBE) for performing the CNS and FTIRS analysis, Maarika Bischof and Daniela Fischer from the Institute of Geography (UniBE) for their help with the PSD analysis, Edith Vogel from the LARA

laboratory (UniBe) for the sample preparation for radiocarbon analysis, and Katrina Kremer from the Institute of Geological Sciences (UniBE) for her advice with the age model. We are grateful to two anonymous reviewers who provided constructive and helpful comments on the first version of the manuscript.

**Author contributions** DP wrote the main manuscript text and prepared all the figures as part of his master thesis, which was supervised and supported by FA. FG and TK. collected the surface sediment samples. JH carried out the GPR survey and provided input to the geophysical methods, results and data interpretation sections. HV processed the FTIRS raw data and provided input to the geochemical methods, results and data interpretation sections. SSc provided input to the sediment-core data processing and interpretation. SSz coordinated the AMS  $^{14}\text{C}$  measurements and provided input to the age model method and results sections. SB, HB and UL. provided input to the archaeological background and lake-level changes sections. MW provided input to the site, sediment and interpretation sections. All authors reviewed and approved the final manuscript.

**Funding** Open access funding provided by University of Bern. The project received financial support from the Archaeological Department of the Canton of Thurgau.

**Declarations**



**Conflict of interest** The authors declare that they have no competing interests as defined by Springer, or other interests that might be perceived to influence the results and/or discussion reported in this paper.

**Open Access** This article is licensed under a Creative Commons Attribution 4.0 International License, which permits use, sharing, adaptation, distribution and reproduction in any medium or format, as long as you give appropriate credit to the original author(s) and the source, provide a link to the Creative Commons licence, and indicate if changes were made. The images or other third party material in this article are included in the article's Creative Commons licence, unless indicated otherwise in a credit line to the material. If material is not included in the article's Creative Commons licence and your intended use is not permitted by statutory regulation or exceeds the permitted use, you will need to obtain permission directly from the copyright holder. To view a copy of this licence, visit <http://creativecommons.org/licenses/by/4.0/>.

## References

- Benguereel S, Ebersbach R, Königer J, Mainberger M, Million S, Nelle O, Schnyder M (2020) Der Bodenseeausfluss als Siedlungsraum. In: Benguerel S et al (eds) *Der Orkopf. Eine Fundstelle auf der Landesgrenze. Archäologie im Thurgau 20. Siedlungsarchäologie im Alpenvorland XIV, 22–23*, Departement für Erziehung und Kultur des Kantons Thurgau, Frauenfeld, pp 209–234
- Billamboz A (2014) Regional patterns of settlement and woodland developments: dendroarchaeology in the Neolithic pile-dwellings on Lake Constance (Germany). *Holocene* 24:1278–1287. <https://doi.org/10.1177/095963614540956>
- Blaauw M, Christen JA (2011) Flexible paleoclimate age-depth models using an autoregressive gamma process. *Bayesian Anal* 6:457–474. <https://doi.org/10.1214/11-BA618>
- Brem H, Leuzinger U (2016) Archaeology and in situ preservation in Canton Thurgau, Switzerland. *Conserv Manag Archaeol Sites* 18(1–3):276–286
- Clark PU, Shakun JD, Baker PA, et al. (2012) Global climate evolution during the last deglaciation. *Proc Natl Acad Sci USA* 109: E 1134–E1142. <https://doi.org/10.1073/pnas.1116619109/-DCSupplemental>
- Dieckmann B, Maier U, Vogt R (1997) Hornstaad-Hörnle, eine der ältesten jungsteinzeitlichen Pfahlsiedlungen am Bodensee. In: Schlichtherle H (ed) *Pfahlbauten rund um die Alpen*. Theiss, Stuttgart, pp 15–21
- Ebersbach R, Mainberger M, Goldhammer J, Ostendorp W (2019) Archäologische Denkmalpflege in der Uferzone des Bodensees. In: Hofmann H, Ostendorp W (eds) *Seeufer: Wellen–Erosion–Schutz–Renaturierung. Handlungsempfehlungen für den Gewässerschutz—Ergebnisse aus dem ReWaM-Verbundprojekt HyMoBioStrategie (2015–2018)*. Universität Konstanz, Konstanz, pp 119–126
- Förstner U, Müller G, Reineck H-E (1968) Sedimente und Sedimentgefüge des Rheindeltas im Bodensee. *Neues Jb Miner Abh* 109:33–62
- Giovanoli F (1991) Korrelation der lithologischen Einheiten im Bodensee-Untersee mittels reversibler magnetischer Suszeptibilität. *Ber Röm-Ger Komm* 71:264–271
- Güde H, Straile D (2016) *Limnologie Aktuell 15: Bodensee Oekologie und anthropogene Belastungen eines tiefen Voralpensees*. Schweizerbart'sche Verlagsbuchhandlung, Stuttgart
- Hagmann S, Schlichtherle H (2011) UNESCO-Welterbe: Prähistorische Pfahlbauten rund um die Alpen. Ein erfolgreicher internationaler Welterbeantrag mit baden-württembergischer Beteiligung. *Denkmalpflege in Baden-Württemberg, Nachrichtenblatt Der Landesdenkmalpflege* 40:194–201
- Hanisch S, Wessels M, Niessen F, Schwalb A (2009) Late Quaternary lake response to climate change and anthropogenic impact: biomarker evidence from Lake Constance sediments. *J Paleolimnol* 41:393–406. <https://doi.org/10.1007/s10933-008-9232-4>
- Hasenfratz A (1997) Pfahlbauten im südlichen Bodenseeraum. In: Schlichtherle H (ed) *Pfahlbauten rund um die Alpen*. Theiss, Stuttgart, pp 36–41
- Hofmann W (1991) Sukzessionen der Cladoceren- und Chironomidenfauna im Spät- und Postglazial als Reaktion auf Änderungen des Trophiegrades im Untersee (Kern US 8707). *Ber Röm-Ger Komm* 71:286–292
- Hofmann H, Salvarina I, Rothhaupt KO, Wessels M, Ostendorp W (2019) Die Fahrgastschiffahrt als Stressor in der Flachwasserzone von Seen. In: Hofmann H, Ostendorp W (eds) *Seeufer: Wellen–Erosion–Schutz–Renaturierung: Handlungsempfehlungen für den Gewässerschutz: Ergebnisse aus dem ReWaM-Verbundprojekt HyMoBioStrategie (2015–2018)*. Universität Konstanz, Konstanz, pp 97–116
- Hornung J (2018) Unterwasser-Georadaruntersuchungen an den “Hügeli” offshore vor Uttwil, Güttingen und Romanshorn. Bodensee, Kanton Thurgau, Schweiz. Unpublished Research Report. Technische Universität Darmstadt, Darmstadt
- Hornung J (2023) Submersible ground penetrating radar (SGPR)—chances and limits for underwater investigations. In: *Advances in on- and offshore archaeological prospection: Proceedings of the 15<sup>th</sup> International Conference on Archaeological Prospection*. Universitätsverlag Kiel, Kiel University Publishing, pp 21–24. <https://doi.org/10.38072/978-3-928794-83-1/p3>
- Internationale Gewässerschutzkommission für den Bodensee (IGKB) (2016) *Bodensee–Untersuchung–Seeboden*. Forschungsprojekt von 2003 bis 2006. Blaue Reihe, Bericht Nr. 56
- Jacomet S, Leuzinger U, Schibler J (2004) Die Jungsteinzeitliche Seeufersiedlung Arbon-Bleiche 3. Umwelt und Wirtschaft. *Archäologie im Thurgau* 12. Departement für Erziehung und Kultur des Kantons Thurgau, Frauenfeld
- Kamleitner S, Ivy-Ochs S, Manatschal L et al (2023) Last Glacial maximum glacier fluctuations on the northern Alpine foreland: geomorphological and chronological reconstructions from the Rhine and Reuss glacier systems.

- Geomorphology 423:108548. <https://doi.org/10.1016/j.geomorph.2022.108548>
- Keller O (1994) Entstehung und Entwicklung des Bodensees—Ein geologischer Lebenslauf. In: Maurer H (ed) Umweltwandel am Bodensee. UVK Fachverlag für Wissenschaft und Studium GmbH, St. Gallen, pp 33–91
- Kober B, Schwab A, Schettler G, Wessels M (2007) Constraints on paleowater dissolved loads and on catchment weathering over the past 16 ka from  $^{87}\text{Sr}/^{86}\text{Sr}$  ratios and Ca/Mg/Sr chemistry of freshwater ostracode tests in sediments of Lake Constance, Central Europe. *Chem Geol* 240:361–376. <https://doi.org/10.1016/j.chemgeo.2007.03.005>
- Kolb M (1997) Die Seeufersiedlung Sipplingen und die Entwicklung der Horgener Kultur am Bodensee. In: Schlichtherle H (ed) Pfahlbauten rund um die Alpen. Theiss, Stuttgart, pp 22–28
- Königer J (1997) Ufersiedlungen der frühen Bronzezeit am Bodensee. In: Schlichtherle H (ed) Pfahlbauten rund um die Alpen. Theiss, Stuttgart, pp 29–35
- Leuzinger U, Anselmetti F, Benguerel S, Degel C, Ehman H, Gilliard F, Hipp R, Hornung J, Keiser T, Müller E, Muigg B, Nigg V, Perler D, Schnyder M, Sturm M, Szidat S, Tegel W, Wessels M, Brem H (2021) “Hügel” im Bodensee—Rästelhafte Steinschüttungen in der Flachwasserzone zwischen Romanshorn und Altnau, Kanton Thurgau (Schweiz). *Jahrbuch Archäologie Schweiz* 104:101–116
- Leuzinger U (2010) Alt- und Mittelsteinzeit. In: Amt für Archäologie Thurgau (ed) Archäologie im Thurgau. Archäologie im Thurgau 16. Huber, Frauenfeld/Stuttgart/Wien, pp. 67–83
- Leuzinger U et al (2013) (eds) Römer, Alamannen, Christen. Frühmittelalter am Bodensee. Frauenfeld
- Magny M (2004) Holocene climate variability as reflected by mid-European lake level fluctuations and its probable impact on prehistoric human settlements. *Quat Int* 113:65–79. [https://doi.org/10.1016/S1040-6182\(03\)00080-6](https://doi.org/10.1016/S1040-6182(03)00080-6)
- Magny M (2007) Holocene fluctuations of lake levels in west-central Europe: methods of reconstruction, regional pattern, palaeoclimatic significance and forcing factors. In: Elias SA, Mock CJ (eds) *Encyclopedia of Quaternary Science*. Elsevier, Amsterdam, pp 1389–1399
- Magny M, Haas JN (2004) A major widespread climatic change around 5300 cal. yr BP at the time of the Alpine Iceman. *J Quat Sci* 19:423–430. <https://doi.org/10.1002/jqs.850>
- Magny M, Leuzinger U, Bortenschlager S, Haas JN (2006) Tripartite climate reversal in Central Europe 5600–5300 years ago. *Quat Res* 65:3–19. <https://doi.org/10.1016/j.yqres.2005.06.009>
- Meyer-Jacob C, Vogel H, Boxberg F et al (2014) Independent measurement of biogenic silica in sediments by FTIR spectroscopy and PLS regression. *J Paleolimnol* 52:245–255. <https://doi.org/10.1007/s10933-014-9791-5>
- Meyers PA, Teranes JL (2001) Sediment organic matter. In: Last WM, Smol JP (eds) *Tracking environmental change using lake sediments volume 2: physical and geochemical methods*. Kluwer Academic Publishers, Dordrecht, pp 239–271
- Milan M, Albrecht N, Peeters F, Wengrat S, Wessels M, Straile D (2022) Clockwise hysteresis of diatoms in response to nutrient dynamics during eutrophication and recovery. *Limnol Oceanogr* 67(9):1–13. <https://doi.org/10.1002/lno.12190>
- Müller E (2011) Geologie. In: Benguerel S et al. (eds) *Tasgetium. Das Römische Eschenz. Archäologie im Thurgau 17*, Departement für Erziehung und Kultur des Kantons Thurgau, Frauenfeld, pp 15–25
- Murray MR (2002) Is laser particle size determination possible for carbonate-rich lake sediments? *J Paleolimnol* 27:173–183
- Neukirch S (1991) Pigmente in Sedimenten des Bodensee-Untersees als Indikatoren der Bioproduktion. *Ber Röm-Ger Komm* 71:279–286
- Niessen F, Sturm M (1991) Lithologische Gliederung und Genese der spät- und postglazialen Sedimente des Bodensee-Untersees. *Ber Röm-Ger Komm* 71:248–258
- Niessen F, Lister G, Giovanoli F (1992) Dust transport and palaeoclimate during the Oldest Dryas in Central Europe—implications from varves (Lake Constance). *Clim Dyn* 8:71–81
- Ostendorp W (1991) Stratigraphische und sedimentologische Untersuchungen im Bereich der Station Hörnle I am Bodensee-Untersee. *Ber Röm-Ger Komm* 71:292–304
- Ostendorp W, Peeters F, Hofmann H, Schlichtherle H, Brem H (2016) Erosion hazards and efficient preservation measures in prehistoric cultural layers in the littoral of Lake Constance (Germany, Switzerland). *CMAS* 18:217–229
- Reimer PJ, Austin WEN, Bard E et al (2020) The IntCal20 Northern Hemisphere radiocarbon age calibration curve (0–55 cal kBP). *Radiocarbon* 62:725–757. <https://doi.org/10.1017/RDC.2020.41>
- Ryzak M, Bieganski A (2011) Methodological aspects of determining soil particle-size distribution using the laser diffraction method. *J Soil Sci Plant Nutr* 174:624–633. <https://doi.org/10.1002/jpln.201000255>
- Schaller S, Böttcher ME, Buechi MW et al (2022) Postglacial evolution of Lake Constance: sedimentological and geochemical evidence from a deep-basin sediment core. *Swiss J Geosci* 115:1–25. <https://doi.org/10.1186/s00015-022-00412-1>
- Schlichtherle H (2004) Lake-dwellings in south-western Germany: history of research and contemporary perspectives. In: Menotti F (ed) *Living on the lake in prehistoric Europe: 150 years of lake-dwelling research*. Routledge, New York, pp 2–35
- Schmieder K, Schünemann B, Schröder HG (2004) Spatial patterns of surface sediment variables in the littoral zone of Lake Constance (Germany). *Arch Hydrobiol* 161:455–468. <https://doi.org/10.1127/0003-9136/2004/0161-0455>
- Schwab A, Dean W, Güde H, Hanisch S, Sobek S, Wessels M (2013) Benthic ostracode  $\delta^{13}\text{C}$  as sensor for early Holocene establishment of modern circulation patterns in central Europe. *Quat Sci Rev* 66:112–122. <https://doi.org/10.1016/j.quascirev.2012.10.032>
- Szidat S, Salazar GA, Vogel E, Battaglia M, Wacker L, Synal HA, Türler A (2014)  $^{14}\text{C}$  analysis and sample preparation at the new Bern laboratory for the analysis of radiocarbon

- with AMS (LARA). Radiocarbon 56:561–566. <https://doi.org/10.2458/56.17457>
- Vogel H, Meyer-Jacob C, Thöle L, Lippold JA, Jaccard SL (2016) Quantification of biogenic silica by means of Fourier transform infrared spectroscopy (FTIRS) in marine sediments. *Limnol Oceanogr Methods* 14:828–838. <https://doi.org/10.1002/lom3.10129>
- Vogt R (2020) Landschaftsraum und geologischer Untergrund im Umfeld des Fundplatzes Orkopf. In: Benguerel S et al (eds) *Der Orkopf. Eine Fundstelle auf der Landesgrenze. Archäologie im Thurgau 20. Siedlungsarchäologie im Alpenvorland XIV*, 22–23, Departement für Erziehung und Kultur des Kantons Thurgau, Frauenfeld, pp 19–25
- Wessels M (1995) Bodensee-Sedimente als Abbild von Umweltänderungen im Spät- und Postglazial. *Gött Arb Geol Paläontol* 66:1–105
- Wessels M (1998c) Natural environmental changes indicated by Late Glacial and Holocene sediments from Lake Constance, Germany. *Palaeogeogr Palaeoclimatol Palaeoecol* 140:421–432
- Wessels M (1999) Kleinskalige Variabilität von Wasserbewegungen in der Flachwasserzone am Südufer des Bodensees. *N Jb Geol Paläontol Abh* 214:319–352
- Wessels M, Mohaupt K, Kümmerlin R, Lenhard A (1999) Reconstructing past eutrophication trends from diatoms and biogenic silica in the sediment and the pelagic zone of Lake Constance, Germany. *J Paleolimnol* 21:171–192
- Wessels M, Hornung J (2019) Unterwassergeoradar zur Untersuchung von Sedimenten der Flachwasserzone. In: Hofmann H, Ostendorp W (eds) *Seeufer: Wellen-Erosion-Schutz-Renaturierung. Handlungsempfehlungen für den Gewässerschutz—Ergebnisse aus dem ReWaM-Verbundprojekt HyMoBioStrategie (2015–2018)* Universität Konstanz, Konstanz, pp 33–36. <https://doi.org/10.18148/KOPS/HMBS.2018.001>
- Wessels M, Weber M (2013) Sedimentkerne als Werkzeug zur Abschätzung der Gefährdung von archäologischen Denkmälern in der Flachwasserzone. In: Brem H, Eberschweiler B, Grabher G, Schlichtherle H, Schröder HG (eds) *Erosion und Denkmalschutz am Bodensee und Zürichsee. Ein internationales Projekt im Rahmen des Interreg IV-Programms “Alpenrhein-Bodensee-Hochrhein” zur Entwicklung von Handlungsoptionen zum Schutz des Kulturgutes unter Wasser*. Vorarlberg Museum, Bregenz, pp 105–110
- Wessels M, Anselmetti FS, Baran R, Hilbe M, Gessler S, Wintersteller P (2016) Tiefenschärfe—Hochauflösende Vermessung Bodensee. Bericht Nr. 61, Institut für Seenforschung (ISF) der Landesanstalt für Umwelt, Messungen und Naturschutz Baden-Württemberg (LUBW), Langenargen
- Wessels M (1998a) Geological history of the Lake Constance area. In: Bäumler E, Gaedke U (eds) *Lake Constance. Characterization of an ecosystem in transition*. Archiv Hydrobiol. Schweizerbart'sche Verlagsbuchhandlung, Stuttgart, pp 1–12
- Wessels M (1998b) Late-Glacial and postglacial sediments in Lake Constance (Germany) and their palaeolimnological implications. In: Bäumler E, Gaedke U (eds) *Lake Constance. Characterization of an ecosystem in transition*. Archiv Hydrobiol. Schweizerbart'sche Verlagsbuchhandlung, Stuttgart, pp 411–449
- Zaugg A, Blass A, Wessels M (2008) Blatt 1055 Romanshorn. *Geol. Atlas Schweiz 1:25000, Erläut.* 125, Bundesamt für Landestopografie swisstopo, Wabern

**Publisher's Note** Springer Nature remains neutral with regard to jurisdictional claims in published maps and institutional affiliations.

## Terms and Conditions

Springer Nature journal content, brought to you courtesy of Springer Nature Customer Service Center GmbH (“Springer Nature”). Springer Nature supports a reasonable amount of sharing of research papers by authors, subscribers and authorised users (“Users”), for small-scale personal, non-commercial use provided that all copyright, trade and service marks and other proprietary notices are maintained. By accessing, sharing, receiving or otherwise using the Springer Nature journal content you agree to these terms of use (“Terms”). For these purposes, Springer Nature considers academic use (by researchers and students) to be non-commercial.

These Terms are supplementary and will apply in addition to any applicable website terms and conditions, a relevant site licence or a personal subscription. These Terms will prevail over any conflict or ambiguity with regards to the relevant terms, a site licence or a personal subscription (to the extent of the conflict or ambiguity only). For Creative Commons-licensed articles, the terms of the Creative Commons license used will apply.

We collect and use personal data to provide access to the Springer Nature journal content. We may also use these personal data internally within ResearchGate and Springer Nature and as agreed share it, in an anonymised way, for purposes of tracking, analysis and reporting. We will not otherwise disclose your personal data outside the ResearchGate or the Springer Nature group of companies unless we have your permission as detailed in the Privacy Policy.

While Users may use the Springer Nature journal content for small scale, personal non-commercial use, it is important to note that Users may not:

1. use such content for the purpose of providing other users with access on a regular or large scale basis or as a means to circumvent access control;
2. use such content where to do so would be considered a criminal or statutory offence in any jurisdiction, or gives rise to civil liability, or is otherwise unlawful;
3. falsely or misleadingly imply or suggest endorsement, approval, sponsorship, or association unless explicitly agreed to by Springer Nature in writing;
4. use bots or other automated methods to access the content or redirect messages
5. override any security feature or exclusionary protocol; or
6. share the content in order to create substitute for Springer Nature products or services or a systematic database of Springer Nature journal content.

In line with the restriction against commercial use, Springer Nature does not permit the creation of a product or service that creates revenue, royalties, rent or income from our content or its inclusion as part of a paid for service or for other commercial gain. Springer Nature journal content cannot be used for inter-library loans and librarians may not upload Springer Nature journal content on a large scale into their, or any other, institutional repository.

These terms of use are reviewed regularly and may be amended at any time. Springer Nature is not obligated to publish any information or content on this website and may remove it or features or functionality at our sole discretion, at any time with or without notice. Springer Nature may revoke this licence to you at any time and remove access to any copies of the Springer Nature journal content which have been saved.

To the fullest extent permitted by law, Springer Nature makes no warranties, representations or guarantees to Users, either express or implied with respect to the Springer nature journal content and all parties disclaim and waive any implied warranties or warranties imposed by law, including merchantability or fitness for any particular purpose.

Please note that these rights do not automatically extend to content, data or other material published by Springer Nature that may be licensed from third parties.

If you would like to use or distribute our Springer Nature journal content to a wider audience or on a regular basis or in any other manner not expressly permitted by these Terms, please contact Springer Nature at

[onlineservice@springernature.com](mailto:onlineservice@springernature.com)